Research Square

Preprints are preliminary reports that have not undergone peer review.
They should not be considered conclusive, used to inform clinical practice,
or referenced by the media as validated information.

Cell-type-specific QKI signaling drives stromal-epithelial oncogenesis in pancreatic cancer through distinct YAP phosphorylation mechanisms

Guo Chen
Shaanxi Provincial People's Hospital
Yonqquan Bai
Hefei Orthopedic Hospital
Dongsheng Zhai
Fourth Military Medical University
Wenli Zhang
Shaanxi Provincial People's Hospital
Zifan Lu
pharmlzf@163.com
Shaanxi Provincial People's Hospital

Article

Keywords: QKI, pancreatic cancer, cancer-associated fibroblast (CAF), tumor microenvironment, YAP signaling, TNC, FAK/SRC pathway, EMT

Posted Date: September 7th, 2026

DOI: https://doi.org/10.21203/rs.3.rs-10570659/v1

License: This work is licensed under a Creative Commons Attribution 4.0 International License.
Read Full License

Additional Declarations:
No competing interests reported.

Tables 1 is available in the supplementary files section.

Cell-type-specific QKI signaling drives stromal-epithelial oncogenesis in pancreatic cancer through distinct YAP phosphorylation mechanisms

Guo Chen[1], Yongquan Bai[2], Dongsheng Zhai[3], Wenli Zhang[1], Zifan Lu[1 *]

1 Translational Medicine Center, Shaanxi Provincial People's Hospital, Xi'an, China.

2 Hefei Orthopedic Hospital, He fei, , China

3 State Key Laboratory of Cancer Biology, Department of Biopharmaceutics, Air Force Medical University, Xi'an, China.

*Correspondence: Zifan Lu Emai:pharmlzf@163.com

Abstract

Background: Cancer-associated fibroblasts (CAFs) are integral to the tumor microenvironment, particularly in pancreatic ductal adenocarcinoma (PDAC), where they constitute about 80% of the tumor mass. Their influence on cancer initiation, progression, and metastasis is significant, yet the detailed mechanisms of their interaction with PDAC are not fully understood.

Methods: Our study focused on the Quaking protein (QKI), an RNA-binding protein implicated in epithelial-to-mesenchymal transition (EMT) through the FAK/SRC signaling pathway. We investigated QKI's role in CAFs by examining its direct interaction with TNC, leading to YAP^{Y357} phosphorylation. Conversely, in cancer cells, we studied how QKI downregulates α-catenin, thereby suppressing YAP^{S127} phosphorylation.

Results: We discovered that QKI plays a dual role in modulating the tumor microenvironment. In CAFs, QKI interacts with TNC, promoting YAP^{Y357} phosphorylation, which is distinct from its suppressive effect on YAP^{S127} phosphorylation in cancer cells via α-catenin downregulation. These mechanisms contribute to the intricate process of oncogenesis.

Conclusions: Our findings reveal QKI as a pivotal mediator in the dialogue between cancer cells and CAFs. Targeting this interaction could lead to the development of novel therapeutic strategies for PDAC patients, potentially offering a new avenue for treatment.

Keywords

QKI, pancreatic cancer, cancer-associated fibroblast (CAF), tumor microenvironment, YAP signaling, TNC, FAK/SRC pathway, EMT

Introduction

Pancreatic ductal adenocarcinoma (PDAC) is the fourth leading cause of cancer-related deaths worldwide, with a 5-year survival rate of only 13%[1]. Alarmingly, PDAC is projected to become the second leading cause of cancer-related deaths by 2030 [2]. Due to its heterogeneity and lack of specific genetic markers, pancreatic cancer is often detected at an advanced stage, complicating the development of targeted therapies and resulting in a poor prognosis. Despite advances in treating other major cancers, pancreatic cancer remains a formidable challenge, as most treatment regimens are ineffective in improving patient outcomes [3; 4]. PDAC is characterized by pronounced desmoplasia, comprising up to 90% of the tumor volume, and a stroma primarily composed (around 90%) of cancer-associated fibroblasts (CAFs) [5].

CAFs secrete soluble factors and extracellular matrix (ECM) proteins through physical interactions with cancer cells, and regulate angiogenesis, immunity, and metabolism, all of which promote cancer progression [6; 7]. Moreover, CAFs mediate drug resistance, metastasis and immunosuppression [8; 9], making them attractive targets for anticancer therapies.

Quaking protein (QKI) is an RNA-binding protein first cloned by Ebersole et al. [10]. QKI regulates RNA splicing, nuclear export of target RNAs, protein translation, and RNA stability [11]. There are three major QKI isoforms–QKI-5, QKI-6, and QKI-7–which have distinct C-termini due to alternative splicing [12]. QKI-5 is localised in the nucleus, QKI-6 is distributed throughout the cell, and QKI-7 is mainly cytosolic. Our previous studies showed that aberrant QKI expression is associated with the development and progression of cancers such as colon [13], prostate [14], breast [15], and gastric cancer [16].

In CAFs, the YAP/TAZ signaling pathway is activated in response to cellular stress and mechanical cues [17]. YAP promotes cancer cell invasion and angiogenesis through ECM remodeling, modulating cell-cell and cell-matrix interactions, as well

as the production of secretory proteins. It is also required for the tumor-promoting role of CAFs in matrix remodeling and angiogenesis. The YAP pathway can thus affect tumor progression by regulating both tumor cells and stromal cells in the tumor microenvironment [18].

In this study, we investigated the role of QKI in PDAC tumorigenesis and identified a previously unknown function for QKI in linking pancreatic cancer with YAP/TAZ signaling. Our results indicate that QKI acts as a bidirectional target gene, enhancing the aggressive properties of both CAFs and cancer cells by modulating YAP and TAZ activities via various YAP isoforms. QKI overexpression in CAFs increased YAP^{Y357} phosphorylation, while QKI knockdown in tumor cells affected YAP^{S127} phosphorylation both in vitro and in vivo.

Methods

Patients and clinical samples

Tumor samples were collected from 10 patients with PDAC who underwent surgical resection at the Xi Jing Hospital between 2022 and 2023 after receiving approval from the Ethical Committee of Xi Jing Hospital. Informed consent was obtained from all subjects and/or their legal guardian(s). None of the patients had received radiotherapy, chemotherapy, immunotherapy or targeted therapy before surgery.Tumor samples were collected from 10 patients with PDAC who underwent surgical resection at the Xi Jing Hospital between 2022 and 2023 after receiving approval from the Ethical Committee of Xi Jing Hospital. None of the patients had received radiotherapy, chemotherapy, immunotherapy or targeted therapy before surgery.

Primary cell isolation and culture

Cancer-associated fibroblasts (CAFs) and primary normal fibroblasts (NFs) were isolated from pancreatic ductal carcinoma and corresponding noncancerous tissues. Freshly isolated surgical resections were collected with informed consent from Xi Jing Hospital. For CAF isolation, carcinoma samples were cut (0.5 cm^3) from the core part of PDAC tissues using a sterile scalpel. Some of the isolated specimens were used for histological examination to confirm the diagnosis, and the remaining tissues were minced and dissociated by collagenase digestion

medium (DMEM/F12, collagenase digestion 125units/mg, insulin 10 mg/mL, hydrocortisone 0.5 mg/mL, penicillin 100 U/mL and streptomycin 100 mg/mL) [19]. The sample was digested for 30 min then quenched in 10% FBS/DMEM. Then the dissociated tissues were incubated without shaking plated on a 6-cm dish for 10 min at 37 °C. The stromal cell-enriched supernatant was collected in a new tube and centrifuged at 250 g for 5 min. For NF isolation, similar anatomopathological techniques were used, freshly isolated normal adjacent pancreatic tissue was taken from areas at least 3cm distal to primary PDAC tumor masses [20]. All samples were taken from surgical resections, not from intra surgical biopsies.

Primary fibroblasts were cultured in Dulbecco's modified Eagle's medium (DMEM, GBICO) with 15% fetal bovine serum (FBS, GIBCO) and 1% penicillin/streptomycin at 37 °C in humidified air with 5% CO2.

Cell Lines

The human hepatic stellate cell line LX-2 (Procell, Cat. No. CL-0560), the mouse pancreatic cancer cell line Pan-02 (Procell, Cat. No. CL-0736), the human pancreatic cancer cell line Panc-1 (Procell, Cat. No. CL-0183), and the human pancreatic ductal epithelial cell line HPDE6-7C (SSRCC, Cat. No. JY-J1093) were purchased from these two companies. All cell lines were cultured in the appropriate medium (HyClone, Logan, UT, USA) supplemented with 10% fetal bovine serum (FBS), 100 U/mL penicillin, and 100 μg/mL streptomycin at 37 °C in a humidified incubator with 5% CO_2. Cell line authentication was performed by short tandem repeat (STR) profiling within the last one year and the profiles were matched to reference databases ATCC or DSMZ. Mycoplasma contamination was routinely monitored using a Mycoplasma PCR Detection Kit (Applied Biological Materials, Cat. No. G238) every two, and all cell lines tested negative.

MEF

MEFs were isolated from embryos at 13.5 days post-coitum obtained from timed-pregnant C57BL/6 females bred in-house.Primary mouse embryonic fibroblasts (MEFs) were isolated at 13.5 days post-conception from C57BL/6 mouse embryos as previously described[19]. Briefly, embryos were decapitated, thoroughly minced, and trypsinized in 1 ml of 0.05% Trypsin/0.53 mM EDTA (Gibco/BRL) for

20 min at 37ºC. Ten ml of complete medium [Dulbecco's modified Eagle's medium (DMEM) supplemented with 10% fetal bovine serum (FBS), 2 mM glutamine, 100U/mL penicillin, and 100 μg/mL streptomycin (Gibco/BRL)] was used to inactivate the trypsin and resuspend the dissociated cells. Cells were plated on a 10cm plate and cultured in a 37º C /5% CO2 incubator. These "passage 1" cells were further propagated using a defined 3T3 passaging protocol (i.e. 3 x 10^5 cells were plated per 60 mm dish every 3 days). For all experiments early passage primary MEFs (<5) were used. To immortalize MEFs, cells were passaged according to the 3T3 protocol continuously until growth rates in culture resumed the rapid rates seen in early passage MEFs (i.e. Passage 25 cells and beyond)[21].Cells were cultured in DMEM with 10% FBS, 1% antibiotics, and maintained at 37°C in a humidified incubator of 5% CO2 and 95% air.

QKI5，QKI6 Silencing or Overexpression in MEF,LX2 and PAN02 Cells

The construction of the shQKI5, shQKI6, QKI5 and QKI6 overexpression plasmid and virus packaging were described in our previous study. In brief, cells were adjusted to the appropriate concentration so that they reached 50% confluence at the time of infection. Complete RPMI-1640 medium containing 8 μg/ml polybrene (Santa Cruz Biotechnology) was added. Then the plasmid, and lentiviral particles with empty vector were added separately to different wells and mixed gently. Growth medium was then replaced after 24h. To select transfected cells, puromycin (4 μg/ml, for siQKI ,InvivoGen) or blasticidin (2 μg/ml, for QKI overexpressed cells,InvivoGen) was added to the medium. The effects of silencing or overexpressing QKI in the infected cells were then tested by western blotting.

Cell viability assay

Cell viability was measured using a CCK8 Cell Counting Kit (K1018，Apexbio, USA) according to the manufacturer’s instructions.

Transwell migration and invasion assays

The transwell chamber (Millipore, USA) was used for migration and invasion assays. To evaluate cell migration, cells (2.5×10^4 cells) were seeded in the upper chamber without serum, and the lower chamber was full of conditional medium for different groups. To evaluate cell invasion, the chamber was pre-coated with

Matrigel (BD, USA). Then, cells (2.5×10^4 cells) were seeded in the upper chamber without serum, and the lower chamber was full of conditional medium for different groups. Cells were allowed to migrate or invade for 24 h, then fixed with 4% paraformaldehyde for 10 min and stained with crystal violet at room temperature. The migration or invasion cells were photographed by a light microscope (Leica, Germany). Five random fields (400×) were selected and the number of migration or invasion cells were counted[22]. All samples were conducted with three repeats.

Wound healing assay

PDAC cells with indicated treatments were seeded into 6-well plates. After 24 h, each well was wounded with a 20μl pipette tip. The cell migration was photographed with an inverted microscope at the time points of 0 and 36 h. Three different independent experiments were performed.

Enzyme-linked immune sorbent assay (ELISA) Test

The conditional medium was collected and centrifuged at 1500 rpm for 5 min to remove particles, and the supernatants were frozen at -80 °C until usesd. The production of CTGF in the supernatants was assessed by ELISA using a commercially available ELISA kit (E-EL-M0340c, Elabscience, Houston, TX) according to the manufacturer's recommendations. CTGF(E-EL-H0828c, Elabscience,Houston,TX),PDGF-α(E-EL-H1575c,Elabscience,Houston,TX),MMP2(E-EL-M0780c,H1575c,Elabscience,Houston,TX)、TGF-β、IL-6(E-EL-M0044c, Elabscience, Houston,TX)、LIF(E-EL-H0094c, Elabscience, Houston,TX)

Tube formation assay

Tube formation assay was performed in matrigel that provides the substrate necessary to study angiogenesis in vitro, as described previously[2]. 96-well Plate was coated with growth factor reduced matrigel (40 μl/well) under chilling condition and incubated for solidification at 37 °C for 30 min. HUVECs (5×10^4 cells/well) were harvested and suspended in conditional medium for different groups, plated on the polymerized Matrigel and cultured at 37 °C for 48 h. Tube-like structures were photographed using microscopy. The number of tubes was counted in eight

random microscope fields, and the lengths of the enclosed tube network were measured by Image-Pro Plus software (Media Cybernetics, Inc., Rockville, MD, USA).

Oil red O assay

Lipid staining was performed on frozen-fixed liver tissue sections using iso-propanol method. Briefly, sections were rinsed with 60% iso-propanol and stained with freshly prepared Oil Red O solution for 15 min. Slides were rinsed twice with 60% iso-propanol and nuclei were lightly stained using hematoxylin solution. Slides were washed, mounted, and observed under bright-field microscope.

RNP IP

The immunoprecipitation of endogenous ribonucleoprotein complexes was analyzed using Magna RIP™ RNA-Binding Protein Immunoprecipitation Kit (Sigma, 17-700) according to the manufacturer's instructions.

Immunohistochemistry (IHC) and Immunofluorescence (IF).

For immunofluorescence staining, cells cultured on a 24-well plate were fixed for 20 min in 4% paraformaldehyde. Then, the cells were incubated with primary antibody and Alexa Fluor 488/594-labeled secondary antibodies (Thermo Fisher Scientific). The details of the primary and secondary antibodies are provided in (SUPPLE.files: Table S1). Nuclei were detected with DAPI (4′,6-diamidino-2-phenylindole) media and visualized using EVOS fluorescence microscopy (Thermo Fisher Scientific).

RNA isolation and real-time PCR assay

Total RNA was extracted with Trizol reagent (Invitrogen, USA), and then reverse transcription was performed using the HiScript II Q RT SuperMix kit for qPCR (Vazyme, R223) according to the manufacturer's instructions . qPCR performed using the ChamQ SYBR qPCR Master Mix kit (Vazyme, Q311) in accordance with the manufacturer's instructions. The primers for all PCR primers, and their internal reference sequences were designed using Primer 5 (SUPPLE.files: Table S2). Then, quantitative PCR was performed using a real-time PCR machine (Roche, LightCycler®96). The expression level of each target gene was determined using

β-actin as the normalization control. Relative gene expression was calculated using the $2^{-\Delta\Delta Ct}$ method. Every experiment was repeated at least three times independently.

Western blot analysis

Total protein was extracted using RIPA Lysis Buffer (Beyotime, Guangzhou, China), and the protein concentration was determined using a BCA protein assay kit (Pierce, Rockford, USA) according to the manufacturer's instructions. Then, a western blot assay was performed as previously described. The primary antibodies used are listed in (SUPPLE.files: Table S1). The protein expression was visualized by enhanced chemiluminescence (Millipore, USA). Images were captured using a ChemiDoc XRS imaging system (Bio-Rad, USA), and Quantity One image software was used for the densitometry analysis of each band; β-actin and GAPDH was used as an internal loading control.

Isolation and culture of human pancreatic stellate cells

Normal pancreatic tissues (1.0–1.5 g) obtained from patients undergoing a pancreatic partial resection for benign pancreatic conditions at the First Affiliated Hospital
of forth military university were immediately collected in sterile ice-cold Hanks balanced salt solution (HBSS) containing 100 U/ml penicillin and 100 μg/ml streptomycin (Gibco). The histological diagnostic assessment of specimens was confirmed by pathologists. Human pancreatic stellate cells (PSCs) were isolated using a density gradient method as previously described. Isolated PSCs were maintained at 37 °C with 5% CO2 in DMEM/F12 (HyClone, Logan, USA) medium supplemented with 10% heat-inactivated fetal bovine serum (FBS) (HyClone), 100 U/ml penicillin and 100 μg/ml streptomycin. PSCs were identified by oil red staining of intracellular fat droplets and immunofluorescence of α-smooth muscle actin (α-SMA). Cells cultured in the above medium conditions for 24 h were used in additional experiments.

Luciferase reporter assay

The TNC wild-type or mutant plasmids and QKI mimic were co-transfected into CAFs cells. Then the transfected Cells were seeded into 96-well

plates and luciferase activities were determined by dual luciferase reporter assay system (Promega, USA) according to the manufacturer's instructions.

Flow cytometry

Cells were dispersed as single-cell suspensions with 0.05% trypsin. A total of 1×10^6 cells were collected and stained with Annexin-V-FITC (Sigma,USA) and propidium iodide (PI) (Sigma, USA) for 15 min at room temperature in a dark room. The signal at 488/530 was determined by a FACS LSR Fortessa (BD Biosciences, USA) and analyzed by FlowJo10.7 software. Each sample was done in triplicates.

Soft agar colony formation

using a colony formation assay. the cells (500 cells) were seeded in 6-well plates with conditional medium for different groups for 2 weeks, which was replaced every 3 days.Colonies with >50 cells were then fixed with 4% formaldehyde for 15 min at 37˚C, stained with crystal violet for 10-20 min at 37˚C and counted under a light microscope (Olympus Corporation; magnification, x10). Finally, the data obtained from five stochastic fields were used for the statistical analysis[23].

RNase R digestion and actinomycin D assay

For RNase R digestion assay, total RNA of NFs and CAFs were treated with or without 5 U/μg RNase R (RNR07250, Epicenter Technologies) and incubated at 37℃ for 30 min. For actinomycin D assay, or total RNA was treated with 2 μg/mL actinomycin D (Sigma, USA) for 0 h, 3 h, 6 h and 9 h. And qRT–PCR was used to detected QKI expression levels. The experiments were performed three times.

Conditioned medium derived from human NFs and CAFs

After transfected, matched CAFs were cultured in 25 mL culture flasks at the same density, respectively. The supernatants were harvested after 48 h and centrifuged to removed cell pellets, then the conditioned medium (CM) was stored at -80 °C

Xenograft tumorigenesis assay Mice

C57BL/6, about 8-week mice were purchased from the Animal center of the Fourth Military Medical University and were maintained under a 12-h light/12-h dark cycle at a constant temperature (22°C) with free access to food and water.

Sample size, randomisation, and blinding

A total of 50 mice were used across all animal experiments. The sample size of n = 6 per group was determined *a priori* using G*Power 3.1 software (one-way ANOVA, effect size $f = 0.5$, $\alpha = 0.05$, power = 0.80), which indicated a minimum requirement of $n = 5$ per group; $n = 6$ was allocated to account for potential attrition. Animals were randomly allocated to experimental groups using a computer-generated random number sequence (Microsoft Excel RAND function) by an investigator not involved in outcome assessment. To minimize potential confounders, mice were housed in randomized cage positions with weekly rotation, and the order of tumor measurements and imaging was randomized daily.

Inclusion and exclusion criteria were established a priori. Male BALB/c nude mice, 4 weeks old and weighing 18–22 g, were included. Animals were excluded if they failed to establish palpable tumors by day 30 post-inoculation, if tumor volume exceeded 2,000 mm^3 (humane endpoint), or if severe illness/ulceration occurred. No animals or data points were excluded from the analysis.

Blinding was maintained throughout the study. Investigators performing tumor caliper measurements, IVIS imaging, and histopathological scoring were blinded to group allocation. Group allocation was only revealed to the researcher administering cell injections. The statistician remained blinded to group labels during data analysis.

Subcutaneous implanted model

Pan-02 cells stably overexpressing QKI, MEF cells stably knocking out QKI, and mock cells were injected subcutaneously into 4-week-old male BALB/c nude mice (1×10^6 cells in 100 μL PBS per mouse, $n = 6$ per group). Tumor size was determined by measuring the length and width with a digital caliper, and tumor volume (mm^3) was calculated as $(\text{length} \times \text{width}^2)/2$. Tumor volume was measured every 3 days. All mice were sacrificed 21 days after injection, and tumors from each animal were weighed and examined for histopathological studies.

lung metastasis model

100μL suspension of MEF cells stably knocking out QKI with PAN02 cells and mock The BALB/c mice were randomly divided into three groups, which were were injected into the tail vein with cells from (1) MEFs stably knocking out QKI and

PAN02 cells, (2) MEFs stably transduced with vector and PAN02 cells , (3) PAN02 cells. The mice were imaged with an In Vivo Imaging System (An IVIS Lumina II imaging station) 30 days later. Lung tissues were resected and were examined for metastatic foci via hematoxylin and eosin (HE) staining.

Animal euthanasia

All animal procedures involving nude mice (BALB/c nude) and C57BL/6 mice were performed in strict accordance with the American Veterinary Medical Association (AVMA) Guidelines for the Euthanasia of Animals (2020 Edition). For anesthesia, mice were placed in an induction chamber with isoflurane (3% v/v in 100% oxygen at a flow rate of 1L/min) and maintained with isoflurane (1.5% v/v) via a nose cone during [surgery/imaging/injection/blood sampling]. The depth of anesthesia was monitored by the absence of the toe-pinch withdrawal reflex. For euthanasia, mice were deeply anesthetized with isoflurane (≥5% v/v) followed by cervical dislocation (for mice < 150 g) or carbon dioxide (CO_2) inhalation (20% chamber volume/min) followed by cervical dislocation to ensure death. All animal studies were approved by the Institutional Animal Care and Use Committee of the Fourth Military Medical University(Approval No:IACUC-20241370), and all efforts were made to minimize animal suffering and distress.

Orthotopic Allograft Models.

Tumor (0.5×10^6) cells only or in combination with 0.5×10^6 MEFs were orthotopically transplanted in PBS:Matrigel (1:1) into the pancreas of mice. Growth was measured every 3 d until the humane end point. Orthotopic injection was performed by surgery under anesthesia (4% isofluorane) using the same number of cells for injection as in the s.c. model. The mice were imaged with an In Vivo Imaging System (An IVIS Lumina II imaging station) 30 days later. Mice were killed 4 wk post injection. Tumors were measured by caliper and calculated as length × $\text{width}^2/2$

Tumor imaging

IR-780 was intraperitoneally injected into tumor-bearing nude mice (1μmol/kg). Twenty-four hours after the injection, the mice were anesthetized with pure oxygen containing 2% isoflurane at a flow rate of 1.5 L/min. An IVIS Lumina II imaging

station (Caliper Life Sciences, USA) was used to observe the uptake of IR-780 by PDAC tumors and tumor imaging properties with an excitation wave length of 700 nm and an emission wavelength of 750 nm.

Statistical Analysis

All experiments were independently repeated at least three times (biological replicates, n = 3), and data are presented as mean ± standard deviation (SD). Statistical analyses were performed using GraphPad Prism 8.0 (GraphPad Software, San Diego, CA, USA). Comparisons between two groups were assessed by Student's t-test (parametric) or Mann–Whitney U test (nonparametric). Comparisons among multiple groups were analyzed by one-way analysis of variance (ANOVA) followed by Tukey's post-hoc test. Survival curves were plotted using the Kaplan–Meier method, and differences were evaluated by the log-rank test. Correlations between variables were analyzed by two-sided Pearson's correlation coefficient. Multivariate analysis of relative risk was performed by Cox proportional hazards regression. A two-tailed P value < 0.05 was considered statistically significant.

Results

1 QKI is highly expressed in α-SMA-positive PDAC CAFs and associated with poor early prognosis

We conducted a preliminary analysis using The Cancer Genome Atlas (TCGA) dataset to investigate QKI expression. PDAC RNA-seq data were downloaded from TCGA and analysed for differential gene expression. QKI mRNA expression was analysed in a variety of tumors, revealing significant differences between cancerous and corresponding normal tissues (Figure 1A). According to the Gene Expression Profiling Interactive Analysis (GEPIA-2), QKI was highly expressed in PDAC samples (Figure 1B). However, no correlation was observed between the prognosis and pathological stage (Figure S1A, Figure S1B).

The tumor immune single-cell hub (TISCH) is an scRNA-seq database that focuses on tumor microenvironment (TME). TISCH provides detailed cell-type annotations at the single-cell level, enabling exploration of the TME across different cancer types. Within the PAAD microenvironment, QKI was found to be

higher in fibroblasts (Figure 1C). We also performed multiplex quantitative immunofluorescence using a Biomax tissue microarray (HPan-Ade120Sur-01) containing 60 PDAC cores and matched normal adjacent tissues, and verified that QKI was expressed at much higher levels in CAFs than in tumor cells in PDAC samples (Figure 1D). An overview of the entire chip is shown in FigureS1C. CAF expression was higher in tumor tissues than in normal tissues (Figure1E). Interestingly, the QKI expression rate was also higher too (Figure 1F). The 60 patients with PADC were divided into high- and low-QKI expression groups (Table 1). Although QKI expression did not correlate with overall survival, it was inversely correlated with early survival (Figure 1G-H). These findings suggest a significant correlation between QKI gene expression in α-SMA-positive PDAC CAFs and poor early prognosis.

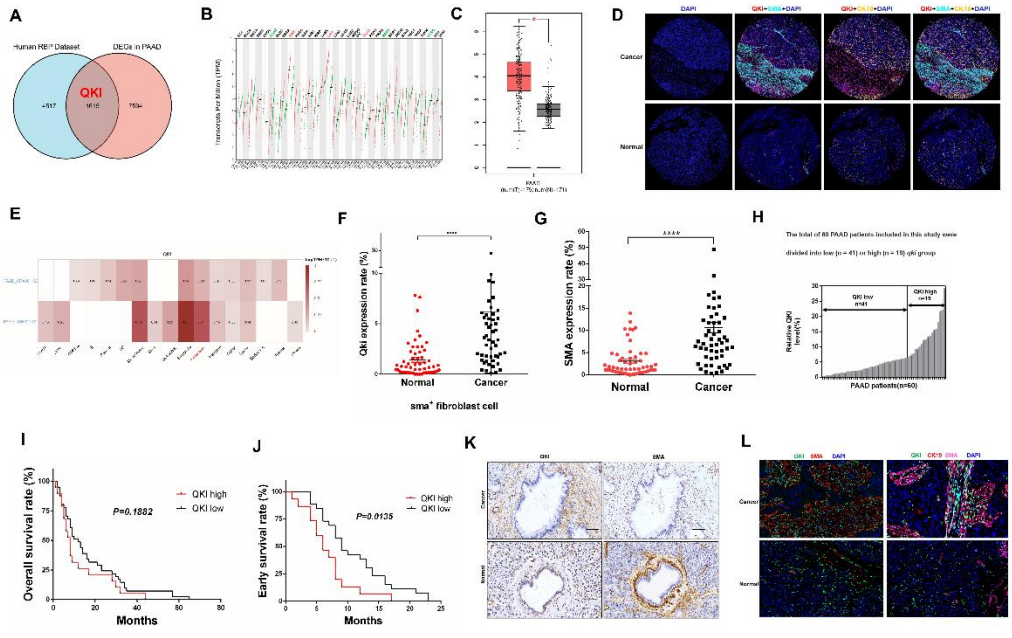


Fig1 QKI is highly expressed in α-SMA-positive PDAC CAFs and associated with poor early prognosis

Fig1A Differential expression of QKI in generalized carcinoma.

Fig1B Differential expression of QKI in PDAC.

Fig1C QKI expression in different cells in PDAC microenvironment by single cell sequencing.

Fig1D Representative IF images of fibroblasts and epithelial cells showing QKI staining

Fig1E Fibroblasts expression in tumor and paracancerous tissues

Fig1F QKI expression in fibroblasts of tumor and paracancerous.

Fig1G Overall survival curves of QKI expression in fibroblasts of PDAC chips .

Fig1H Early survival curves of QKI expression in fibroblasts of PDAC chips.

Fig1I Overall survival curves of QKI expression in fibroblasts of PDAC chips .

Fig1J Early survival curves of QKI expression in fibroblasts of PDAC chips.

Fig1K Representative IHC images showing QKI staining in PDAC samples.

Fig1L Representative IF images of human PDAC showing QKI staining.

Table1 Association between QKI expression and clinicopathological characteristics

Association between QKI expression and clinicopathological characteristics				
Characteristic	No. of patients	Low expression	High expression	P value
Age(years)				0.2574
60	22	17	5	
>60	38	24	14	
Gender				0.3225
Male	34	25	9	
Female	26	16	10	
Tumor size				0.2106
3	8	7	1	
>3	52	34	18	
T stage				0.4277
I+II	24	15	9	
III	36	26	10	
TNM stage				0.6505
I+II	31	22	9	
III	29	19	10	

2 QKI overexpression promotes CAF activation

To evaluate the effects of QKI on fibroblast activation, we used the human stellate cell line LX2. Overexpression of QKI increased protein levels of CAF markers α-SMA, vimentin, and Collagen 1 (Figure 2A-B). Immunofluorescence staining further confirmed these results (Figure 2C-D). mRNA levels were similar to protein

levels (FigureS2A-B), as validated by immunofluorescence (Figure 2E-F). When QKI was overexpressed or knocked down in MEF, mRNA levels of QKI-5, QKI-6, QKI-7, and QKI-common positively correlated with CAF activation markers (Figure S2C-F). Enzyme-linked immunosorbent assay (ELISA) of conditioned media indicated that QKI regulated the expression of these cytokines (Figure2G), with similar alterations observed in cytokine mRNA expression (Figure S2G-H). Morphological differences between normal fibroblasts (NFs) and CAF were observed under light microscopy, where NFs appeared long and fusiform with bundled growth, while CAFs were fat, fusiform with scattered distribution and irregular arrangement (Figure S2I). Oil Red O staining confirmed these morphological differences over several passages (Figure S2J). The mRNA expression of QKI and SMA consistently increased across CAF passages (Figure S2K). These findings suggest that there are positive correlations between QKI and CAF phenotypes and functions.

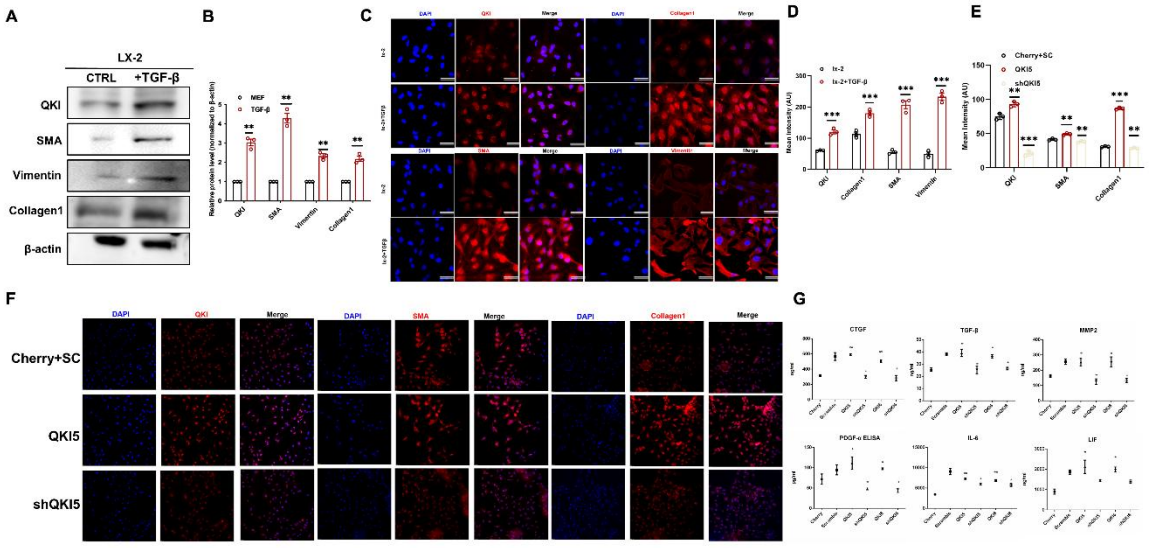


Fig2 QKI overexpression promotes CAF activation

Fig2A-B Western blot analyses showing the expression levels of QKI and CAF markers in LX-2 cells following TGF-β activated for 12 hours.

Fig2C-D Microscopic images of immunofluorescence staining analyses showing the expression levels of QKI and CAF markers in LX-2 cells following TGF-β activated for 12 hours.

Fig2E-F Microscopic images of immunofluorescence staining analysis show that overexpression or knockdown QKI in LX-2 cells had an increased and induced in comparison to shNC group.

Fig2G The ELISA results of activated MEF related cytokine in overexpression or knockdown QKI

3 QKI in CAFs supports PDAC cell proliferation, migration and tumorigenesis

CAFs promote tumor progression partly by supporting the proliferation of PDAC cells [19]. To test this, conditioned media (CM) were collected from MEFs with QKI overexpression or knockdown (Figure 3A). Cell growth was elevated by QKI overexpression, which was inhibited by shQKI, as determined by a cell counting kit-8 assay (Figure 3B). The cell scratch assay demonstrated that the migratory capacity of the cells was attenuated by shQKI (Figure 3C). Transwell invasion assays indicated that the invasiveness of the cells was inhibited by shQKI CAF (Figure 3D). Consistently, HUVEC tube formation was substantially inhibited by the QKI knockdown medium (Figure 3E). Next, we performed soft agar assays which showed similar results to those of the colony formation and proliferation assays (Figure 3F). The results demonstrated that shQKI CAF increased Pan-02 cell apoptosis compared to the corresponding control group (Figure 3G-H). Apoptosis was also detected with the terminal deoxynucleotidyl transferase dUTP nick-end labelling (TUNEL) assay (Figure 3I). Together, these findings suggest an essential role for QKI in CAF in supporting PDAC cell proliferation in vitro.

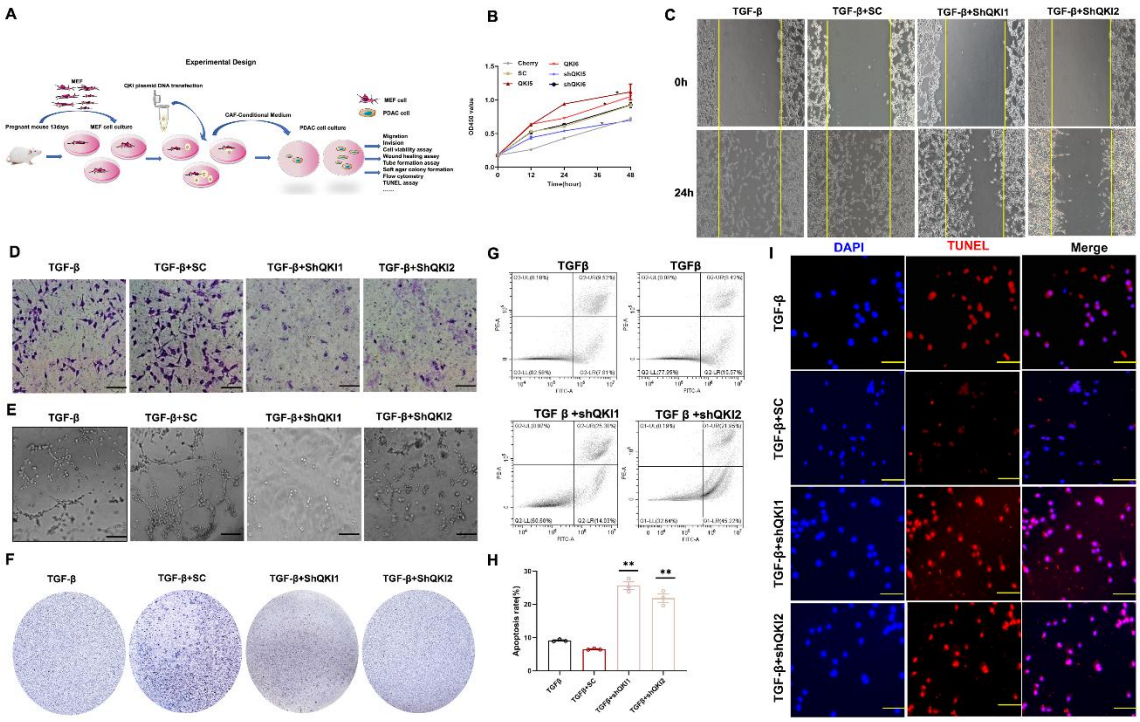


Fig3 QKI in CAFs supports PDAC cell proliferation, migration and tumourigenesis

Fig3A Schematic representation of PDAC cells after treatment with CAF-CM

Fig3B Cell proliferation of PAN-02 cells was detected by CCK-8 assays.

Fig3C-D Wound healing and (C) Transwell (D) invasion assays were performed to detect the effect of QKI overexpression in CAF on migration and invasion

Fig3E Representative pictures of HUVEC tube formation under different CAF CM. Scale bar = 200μm. Quantification of tube formation assessed by the number of tubes and length of tubes.

Fig3F Proliferative tendency of PAN-02 cells were evaluated using soft agar assays.

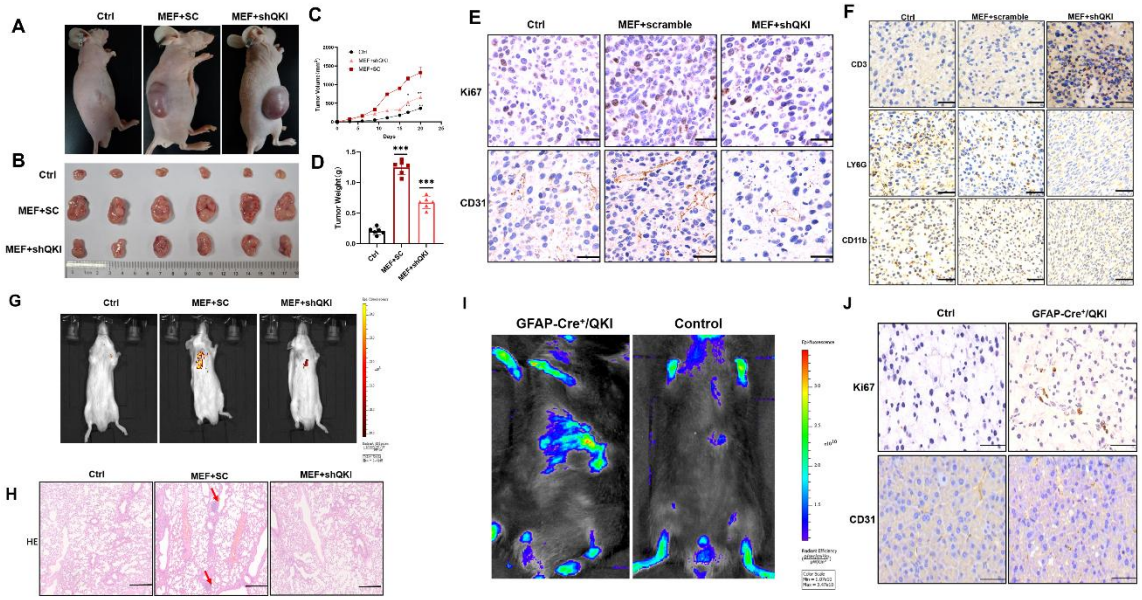
FIG3G-I Annexin V-FITC staining (G-H) and Tunel assay (I) was used to detect apoptosis in PAN-02 cells in the four groups.

4 QKI promotes pancreatic tumorigenesis and metastasis by impacting CAF activation in mouse pancreatic cancer models

CAFs secrete growth factors and cytokines that stimulate the proliferation and migration of tumor cells, as shown in Figure 3. To mimic this process, we collected CM from sh-QKI and sh-NC MEF with TGF-β activation.

To validate these findings in vivo, we constructed xenograft models (Figure S3A-D). Pan-02 cells were co-injected with CAFs expressing either shQKI or control into 4-week-old femalemale BALB/c nude mice (n=8/group), and tumor size was examined. Approximately 21 days later, the tumors were dissected from the tumor-bearing mice. We found that the tumors in the shQKI group were significantly smaller and lighter than those in the control group (Figure 4A-D). Moreover, the dissected neoplasms were embedded in paraffin and assessed by immunohistochemistry; the expression of Ki67 (a proliferative cell marker) and CD31 (a blood vessel endothelial cell marker) in the shQKI group was lower than that in the other groups (Figure 4E).

Immunohistochemistry for CD3, CD11b, and Ly6G indicated that shQKI increased T cell infiltration (CD3+) and reduced myeloid-derived suppressor cell (MDSC) counts compared to controls (Figure.4F). We used an in vivo lung metastasis model to determine whether QKI-CAFs facilitated cancer metastasis. These results suggest that QKI play an important role in PDAC regulation in vivo. According to the bioluminescence images (Figure 4G), shQKI CAF significantly inhibited the progression of lung metastasis. Furthermore, we generated orthotopic allograft tumor models via the intrapancreatic transplantation of pancreatic tumor cells. Haematoxylin and eosin (HE) staining showed a decrease in the number of tumors in the shQKI-CAF group (Figure 4H). Figure 4I illustrates these results. QKI was predominantly expressed in the liver and pancreas (Figure S3E). In addition, QKI co-localisation with SMA was detected using immunohistochemistry (IHC) in the pancreas and liver (Figure S3F). According to the bioluminescence images (Figure 4I) and in situ observation (Figure S3G), GFAP-Cre+/QKI mice exhibited higher tumorigenicity. A higher number of Ki67 and CD31 positive cells were observed in the GFAP-Cre+/QKI group than in the control group (Figure 4J). Taken together, these findings confirm QKI’s essential role in CAF-mediated support of PDAC cell proliferation, both in vivo and in vitro.



498

499 **Fig4 QKI promotes pancreatic tumorigenesis and metastasis by impacting**
500 **CAF activation in mouse pancreatic cancer models**

501 Fig4A-B Representative images of nude mice and subcutaneous tumors.

502 Fig4C-D Volume and Weight measurements of subcutaneous tumors derived
503 from MEF cells stably transfected with pcDNA3.1b (sh-SC) and pcDNA3.1b-shQKI
504 (b).

505 Fig4E Representative images of immunohistochemical staining of CD31 and Ki67
506 in the subcutaneous tumor (a, bar=100 μm) and the Matrigel-plug (b, bar = 20 μm).

507 Fig4F Representative images of immunohistochemical staining of CD3, CD11b
508 and Ly6G in the subcutaneous tumor (a, bar=100 μm) and the Matrigel-plug (b,
509 bar = 20 μm).

510 Fig4G Representative live animal imaging of tumor metastases was detected in
511 the lung.

512 Fig4H H.E. staining of lung metastases tumor.

513 Fig4I Representative images of the lung metastases.

514 Fig4J Representative images of immunohistochemical staining of Ki67 in the
515 primary tumor. Data are representative of three independent experiments. *, $P < 0.05$; **, $P < 0.01$.
516

5.1 QKI promotes CAF activation through SRC/FAK-YAP^{357} Pathway

To investigate the role of QKI in CAF activation, we first treated LX2 cells with commercially available TGF-β. Western blotting was performed to analyse YAP-related signaling pathways, including the SRC, YAP, and EMT pathways. This treatment activated integrin signaling, as evidenced by an increase in phosphorylated-FAK (p-FAK, Tyr397) and SRC (p-SRC, Tyr416). Interestingly, while there was no change in pYAPS127 expression, a significant increase in pYAPY357 expression was observed, indicating that the effect of CAF activation is pYAPY357 -dependent. CAF activation promoted alterations in EMT markers (Figure 5.1A-B). To confirm the effects of SRC and FAK inhibition on CAF activation, the small-molecule inhibitors, Dasatinib and Defactinib, were used to inhibit SRC and FAK kinase activity, respectively. The results shown in (Figure 5.1C-D) supported our hypothesis. Overexpression or knockout of QKI in CAF resulted in changes in p-FAK, p-SRC, pYAP^{Y357}, and EMT marker protein levels (Figure 5.1E-F). The induced expression of pYAP^{Y357} was significantly decreased by the SRC inhibitor (dasatinib) in QKI-overexpressing CAF, whereas the expression of pYAP^{S127} protein was not significantly affected. The same situation was observed with the FAK inhibitor (defactinib) (Figure 5.1G-H). To validate these observations, we performed immunofluorescence staining for QKI overexpression in CAF (Figure 5.1I). Knockout of QKI in CAF resulted in the opposite result of immunofluorescence staining (Figure 5.1J). We also evaluated changes in the TGF-β1/Smad pathway, which regulates collagen synthesis, and observed corresponding protein changes in this pathway (Figure S4A). Additionally, we analyzed CAF activation after the addition of Narciclasine(an RHOA inhibitor), in QKI-overexpressing cells, where protein levels were lower than in control groups (Figure S4B). In summary, we confirmed that QKI enhances CAF activation via the SRC/FAK-YAP357 pathway.

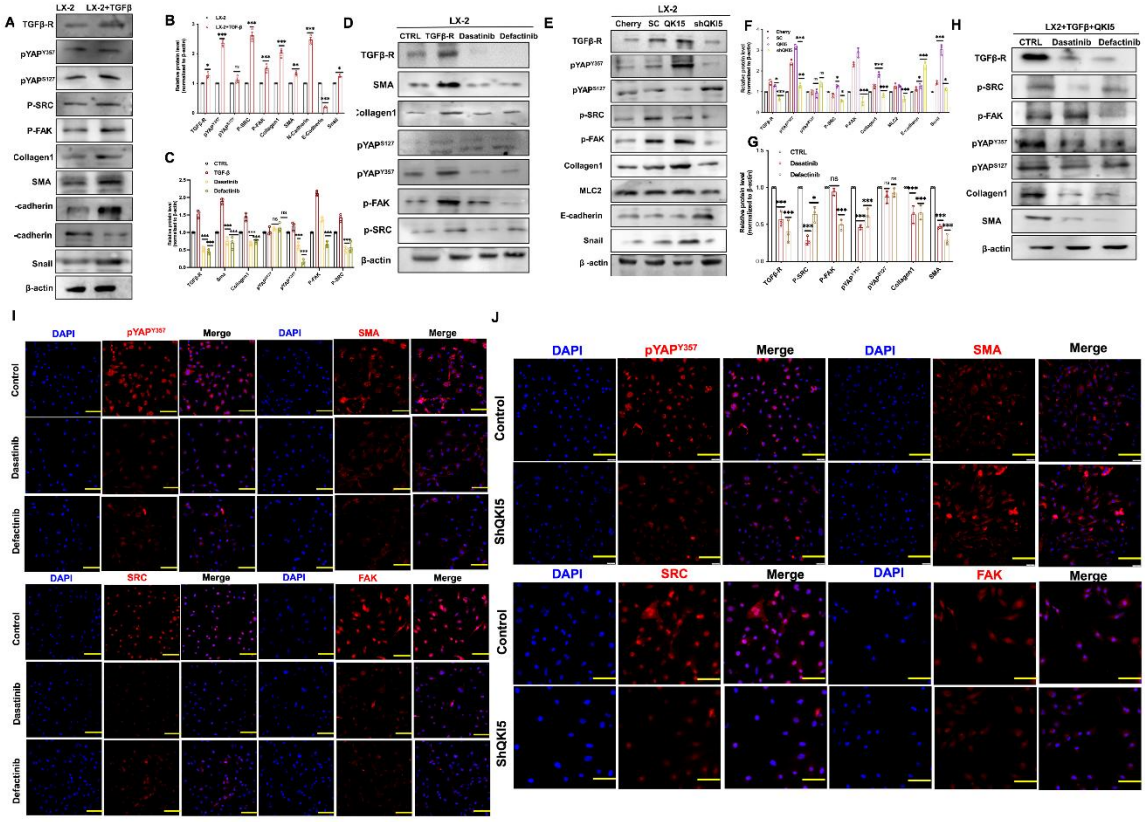


Fig5.1 QKI promotes CAF activation through SRC/FAK-YAP^{357} Pathway

Fig5.1A-B CAF activation affected the protein expression of SRC, FAK, pYAP^{Y357} and EMT

Fig5.1C-D The SRC and FAK inhibitors was used after CAF activation, which affected the protein expression of pYAP^{Y357} and EMT

Fig5.1E-F Silencing or overexpressing QKI in CAF affected the protein expression of pYAP^{Y357} and EMT

Fig5.1G-H The SRC and FAK inhibitors was used in CAF overexpressed QKI, then the protein expression of pYAP^{Y357} and the activation of CAF were affected

Fig5.1I The immunofluorescence of pYAP^{Y357}、SRC、FAK, CAF activation ability in CAF knockdown QKI.

Fig5.1J The immunofluorescence of CAF activation and pYAP^{Y357} by the SRC and FAK inhibitors been used in QKI-overexpressed in CAF.

5.2 QKI enhances signaling and CAF activation by regulating TNC-RNA transport

Proteomic analysis of QKI-overexpressing CAFs identified proteins interacting with QKI. Among the top Gene Ontology (GO) terms for Molecular Function (MF), Biological Process (BP), and focal adhesion were focal adhesion-related proteins (Figure S4C). Differentially expressed genes (DEGs) were categorized into ten groups, with TNC and ITGA5 involved in the focal adhesion pathway (Figure S4D). KEGG pathway analysis of these genes using DAVID bioinformatics resources highlighted the top 10 enriched pathways, including the focal adhesion pathway (Figure 5.2A). Pathway analysis was conducted using the KEGG database [24, 25].The Venn diagram in (Figure 5.2B) shows the overlap between TCGA RNA-seq and mass spectrometric analysis of QKI in CAF. These include the TNC, ITGAV, and PPP2R5E genes related to the focal adhesion pathway. As shown in the volcano plot (Figure 5.2C), upregulated (red) and downregulated (blue) genes were identified in PAAD ($P < 0.05$, $FDR < 0.01$).

Single-cell data from TISCH revealed that TNC, PPP2R5E, and ITGAV are primarily expressed in fibroblasts within the tumor microenvironment (Figure 5.2D).

The morphological changes induced by QKI in CAF were assessed by examining the actin cytoskeletal organisation using Fitc-labelled phalloidin staining (Figure 5.2E). We also examined YAP fluorescence and actin cytoskeletal organisation using Fitc-labelled phalloidin staining after QKI knockout in MEF (Figure S4E). To determine whether QKI overexpression affected cytoskeletal protein expression in CAF, western blot analysis was performed to confirm that the cytoskeletal protein levels of ITGAV, TNC, and PPP2R5E were notably elevated (Figure 5.2F-G). Importantly, the protein levels of p-FAK, p-SRC, and pYAPY357 were elevated. Knockout of QKI in CAF led to a corresponding decrease in these protein levels (Figure 5.2H-I). Next, we investigated whether TNC, ITGAV, and PPP2R5E could bind directly to the mRNAs of their target QKI by RNA immunoprecipitation (RNA-IP) (Figure 5.2J). Transcriptional inhibition experiments using Actinomycin D showed significant differences in the stability of TNC mRNA upon QKI overexpression and no effect on ITGAV or PPP2R5E (Figure 5.2K) (Figure S4F).

Furthermore, a positive correlation between TNC and QKI in PAAD was predicted using GEPIA analysis (r = 0.58, P = 6.5e-18) (Figure 5.2L). To do this, we used anti-QKI antibody immunofluorescence (red) in combination with cytoskeletal protein RNA in situ hybridisation (green) (Figure5.2M) (FigureS4G). A dual-luciferase reporter assay confirmed that QKI bound to TNC. The results of the assay revealed that QKI markedly increased the luciferase activity of the TNC-wild-type (TNC-wt) group compared to the NC group but had no effect on the luciferase activity of the TNC-mutant (TNC-mut) group (Figure 5.2N) (Figure S4H).

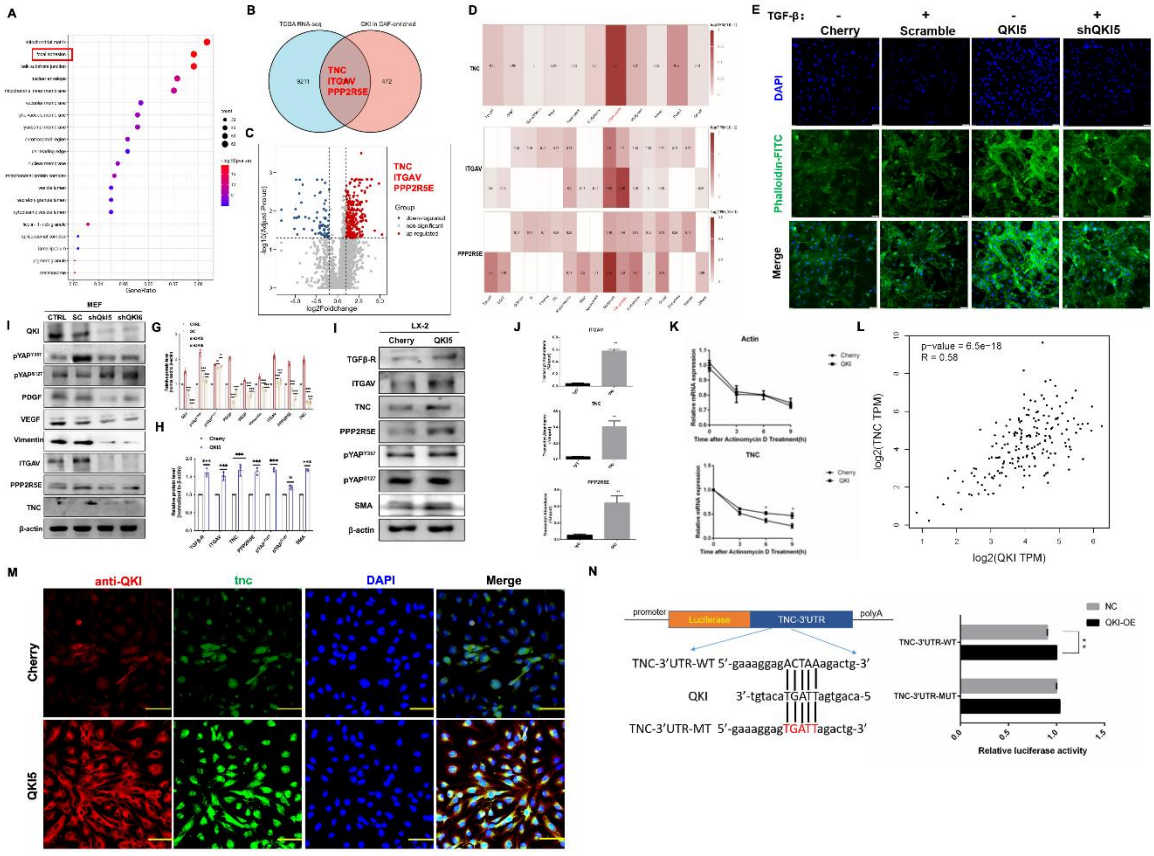


Fig5.2 QKI enhances signaling and CAF activation by regulating TNC-RNA transport

Fig5.2A KEGG pathway analysis of mass spectrometry data. Pathway enrichment was performed using the KEGG database (Kanehisa Laboratories). Reproduced with permission from Kanehisa Laboratories.

Fig5.2B Venn diagram of mass spectrometry: List 1: the RNA-seq differential gene expression of PDAC in TCGA database; list 2: QKI related gene analysis in CAF

Fig5.2C Volcano Plot of differential gene expression of mass spectrometry

Fig5.2D The single-cell transcriptome differential expression of ITGAV,PPP2R5E and TNC in PDAC microenvironment in GSE databases.

Fig5.2E Representative IF images of phalloidin-FITC in the cytoskeleton of CAF affected Silencing or overexpressing QKI

Fig5.2F-G Western blot analysis of ITGA, TNC, PPP2R5E, $pYAP^{Y357}$, SRC and FAK in QKI overexpressed CAF

Fig5.2H-I Western blot analysis of cytoskeletal protein: ITGA, TNC, PPP2R5E, $pYAP^{Y357}$, SRC and FAK in LX-2 cells of QKI knockdown.

Fig5.2J RNA-IP results of cytoskeletal protein TNC, ITGAV and PPP2R5E

Fig5.2K TNC affected the RNA stability of QKI by Actinomycin D

Fig5.2L GEPIA gene correlation analyses between TNC and QKI in PAAD adenocarcinoma.

Fig5.2M RNA-fish results of cytoskeletal protein TNC, and QKI

Fig5.2N Luciferase reporter assay was used to detect the luciferase activity of TNC-WT and TNC-mut (QKI binding site mutated) luciferase reporter cotransfected with QKI.

5.3 QKI promotes tumor development and progression by modulating TNC expression

Knockout of TNC in CAF overexpressing QKI clearly reduced protein levels of CAF activation markers p-FAK, p-SRC, and pYAPY357 (Figure 5.3A-B). This was confirmed by immunofluorescence (Figure5.3C). Interestingly, Dasatinib and Defactinib did not affect TNC (FigureS5C). ELISA analysis of CM from TNC-knockout, QKI-overexpressing CAFs showed decreased secretion of CTGF, TGF-β, PDGF-α, and MMP2 (Figure 5.3D). Knockout of TNC in CAF overexpressing QKI significantly reduced Transwell migration and invasion (Figure 5.2E). Immunofluorescence staining on tumor tissues from a nude mouse model revealed TNC-SMA co-localization, with decreased fluorescence in the shQKI group (Figure 5.3F). To determine whether QKI affects EMT, tumor-bearing tissues were

screened for N-cadherin (an EMT marker). Immunohistochemical staining revealed that CTGF and N-cadherin levels were significantly reduced (Figure 5.3G). Thus, QKI is a novel TNC target gene associated with cancer cell growth and invasion.

In summary, QKI, which influences EMT via the FAK/Src axis, interacts directly with TNC, leading to the activation of YAPY357 phosphorylation in CAFs.

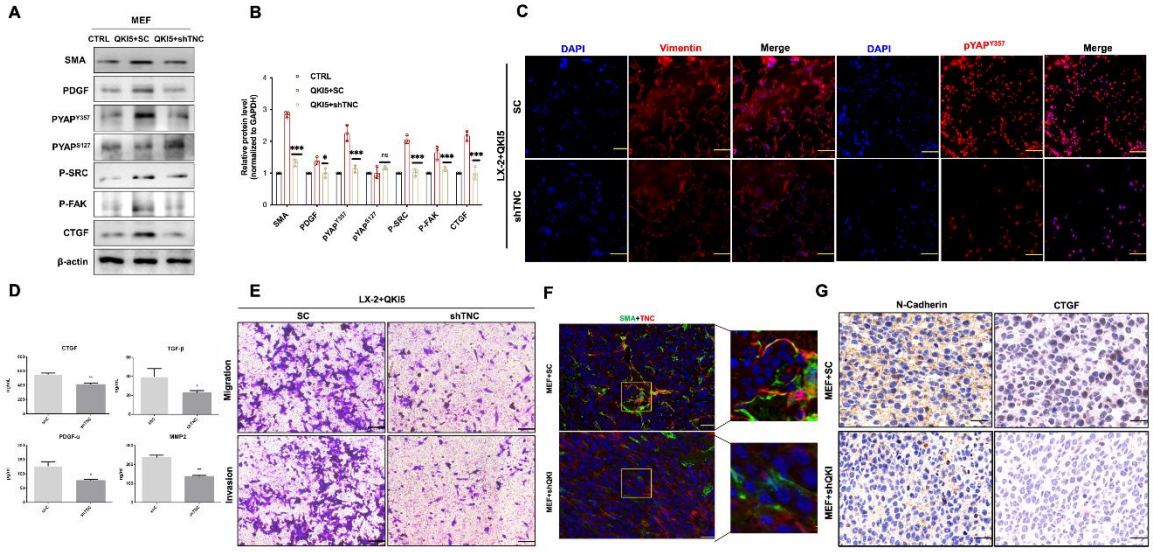


Fig5.3 QKI promotes tumour development and progression by modulating TNC expression

Fig5.3A-B Western blot analysis of SRC, FAK, pYAP^{Y357}, Vimentin, SMA and Collagen in CAF overexpressed QKI before knocking down TNC

Fig5.3C Immunofluorescence analysis of pYAP^{Y357}, Vimentin, SMA and Collagen in CAF overexpressed QKI before knocking down TNC

Fig5.3D ELISA analysis of CAF activation-related cytokines in CAF overexpressed QKI before knocking down TNC

Fig5.3E Overexpression QKI and knockdown TNC in CAF affected the migration and invasion of tumor cells

Fig5.3F Immunofluorescence analysis of TNC / SMA in tumor tissue in vivo xenograft, which was affected by knockdown QKI in CAF

Fig5.3G Multiple immunohistochemistry analysis of CTGF and EMT in tumor tissue

in vivo xenograft, which was affected by knockdown QKI in CAF

6.1 QKI in tumor cells inhibits EMT in PDAC

Interestingly, QKI staining was higher in tumor-bearing nude mice with shQKI CAFs compared to controls. In addition, we performed IHC staining for the phosphorylation of $pYAP^{S127}$ and $pYAP^{Y357}$ and found a striking correspondence that $pYAP^{S127}$ expression was higher in the shQKI CAF group than the control group (Figure 6.1A). Using multiplexed quantitative immunofluorescence of PDAC tissue microarrays, we evaluated QKI protein expression in human pancreatic cancer and normal tissue epithelial samples. QKI expression was lower in tumor tissues than in normal epithelial tissues (Figure 6.1B). We validated our findings in clinical tissue samples using immunofluorescence staining (Figure 6.1C). Pan-02 cancer cells were also treated with CM collected from MEF after QKI overexpression (Figure6.1D-E), and found that QKI protein levels in the QKI overexpression group were lower than those in the control group. pYAPS127 levels was also lower with no change in $pYAP^{Y357}$ expression. CTGF and Snail protein levels were higher than those in the control group. QKI overexpression in pan-02 cells reduced CTGF and EMT markers (N-cadherin, Snail, Twist) and increased a-catenin and $pYAP^{S127}$ protein expression (Figure 6.1F-G). This result was verified using ELISA (Figure 6.1H). QKI overexpression in pan-02 cells reduced CTGF expression, whereas knockout QKI in pan-02 cells significantly recovered CTGF expression. Figure 6.1I-J showed that QKI knockout in pan-02 cells reduced PDGF and VEGF protein levels.

After QKI overexpression or knockout in pan-02 cells, we examined the protein expression levels of α-catenin, $pYAP^{S127}$ $pYAP^{Y357}$, CTGF, and EMT markers (Figure 6.1K-L). In this study, we found that PP2A-C produced corresponding changes, which was confirmed by immunofluorescence (Figure 6.1M). Next, we validated our data in normal pancreatic and tumor cell lines. QKI expression was significantly lower in tumor cells than in normal cells. The expression of CTGF, YAP, and EMT markers also changed accordingly. They were expressed in

normal pancreatic cells, and there was no significant difference in the tumor cells (Figure S5A).

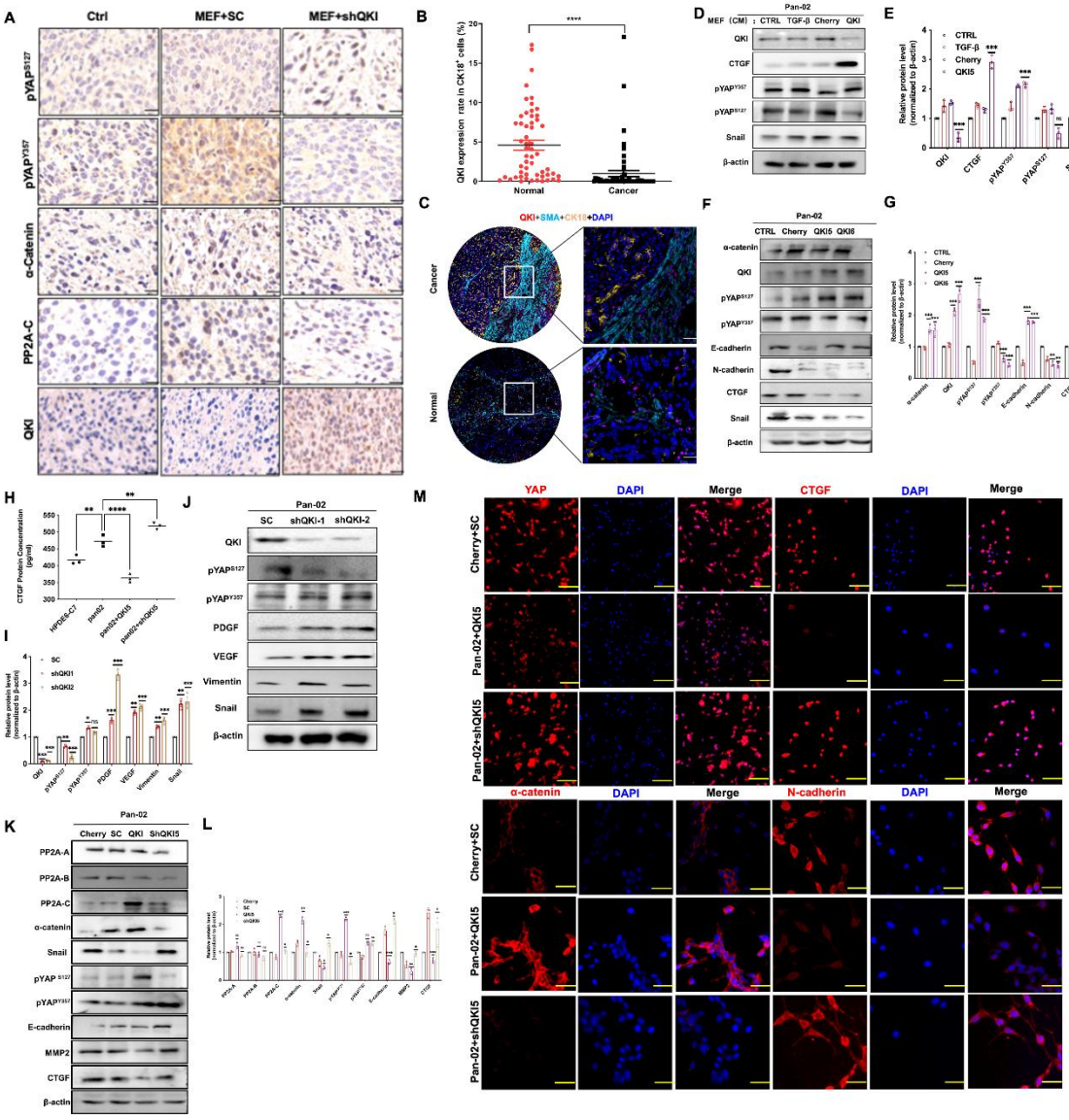


Fig6.1 QKI in tumour cells inhibits EMT in PDAC

Fig6.1A Immunohistochemistry analysis of QKI, PP2A-C and α-catenin in tumor tissue of tumor-bearing nude mice, which was affected by knockdown QKI in CAF

Fig6.1B Different expression of QKI in tumor and normal epithelial tissue chips.

Fig6.1C Immunofluorescence analysis of QKI different expression in tumor and normal epithelial tissue

Fig6.1D-E Western blot analysis of QKI、YAP and EMT in PANC-1 which was co-cultured with Conditional Medium for QKI overexpression in fibroblasts CAF overexpressed QKI.

Fig6.1F-G Western blot analysis of CTGF, a-catenin, $pYAP^{Y357}$, $pYAP^{P127}$ and EMT in PANC-1 cells of QKI overexpressed which secreted by paracrine.

Fig6.1H-I Western blot analysis of paracrine cytokines, YAP and EMT in PANC-1 silenced QKI

Fig6.1J ELISA analysis of CTGF in PANC-1 overexpressed QKI

Fig6.1K-L Western blot analysis of a-catenin, YAP, CTGF and EMT in PANC-1 overexpressed or knockdown QKI

Fig6.1M Immunofluorescence analysis of a-catenin, YAP, CTGF and EMT in PANC-1 overexpressed QKI

6.2 QKI promotes $pYAP^{S127}$ cytoplasmic localization and inactivation through α-catenin

We assessed enzyme expression levels, observing that $pYAP^{S127}$ activation promotes EMT, while YAP promotes pancreatic cancer cell motility, invasion, and tumorigenesis in a phosphorylation-dependent manner and contributes to EMT in pancreatic cancer cells through several mechanisms, including hyperactivation of CTGF[26; 27]. The transfection effect of α-catenin was observed using green fluorescent protein (Figure S5B). The α-catenin silencing effect was confirmed by RT-qPCR (Figure S5C). Knocking out α-catenin in QKI overexpressing pan-02 cells promoted pan-02 cell proliferation (Figure S5D). The protein levels of pYAPS127 and E-cadherin were reduced (Figure 6.2A-B), which was confirmed by immunofluorescence (Figure 6.2C). To test the promotion of pan-02 cell proliferation, we used anti-QKI antibody immunofluorescence (red) in combination with the α-catenin RNA in situ hybridisation (Figure 6.2D). Next, we investigated whether α-catenin is able to bind directly to the mRNAs of its target QKI by RNA immunoprecipitation (RNA-IP) (Figure 6.2E). Transcriptional inhibition experiments using Actinomycin D showed significant differences in the stability of α-catenin mRNA upon QKI knockdown (Figure 6.2F). The results of the assay revealed that QKI markedly decreased the luciferase activity of the α-catenin-wild-

type (α-catenin-wt) group compared to the NC group but had no effect on the luciferase activity of the α-catenin-mutant (α-catenin-mut) group (Figure 6.2G).

To confirm the functions of QKIs in vivo, we constructed a xenograft mouse model. QKI-overexpressing Pan-02 cells were subcutaneously injected into 4-week-old femalemale BALB/c nude mice (n=8/group), and tumor size was examined. Approximately 21 days later, the tumors were dissected from the tumor-bearing mice. The tumors in the QKI group were significantly smaller and lighter than those in the control group (Figure 6.2H). Moreover, the dissected neoplasms were embedded in paraffin and assessed by immunohistochemistry, finding that the expression of α-catenin, CTGF, and N-cadherin in the QKI group were lower than other groups. Additionally, the expression of pYAP^{S127} was higher in the QKI group than in the control group (Figure 6.2I).

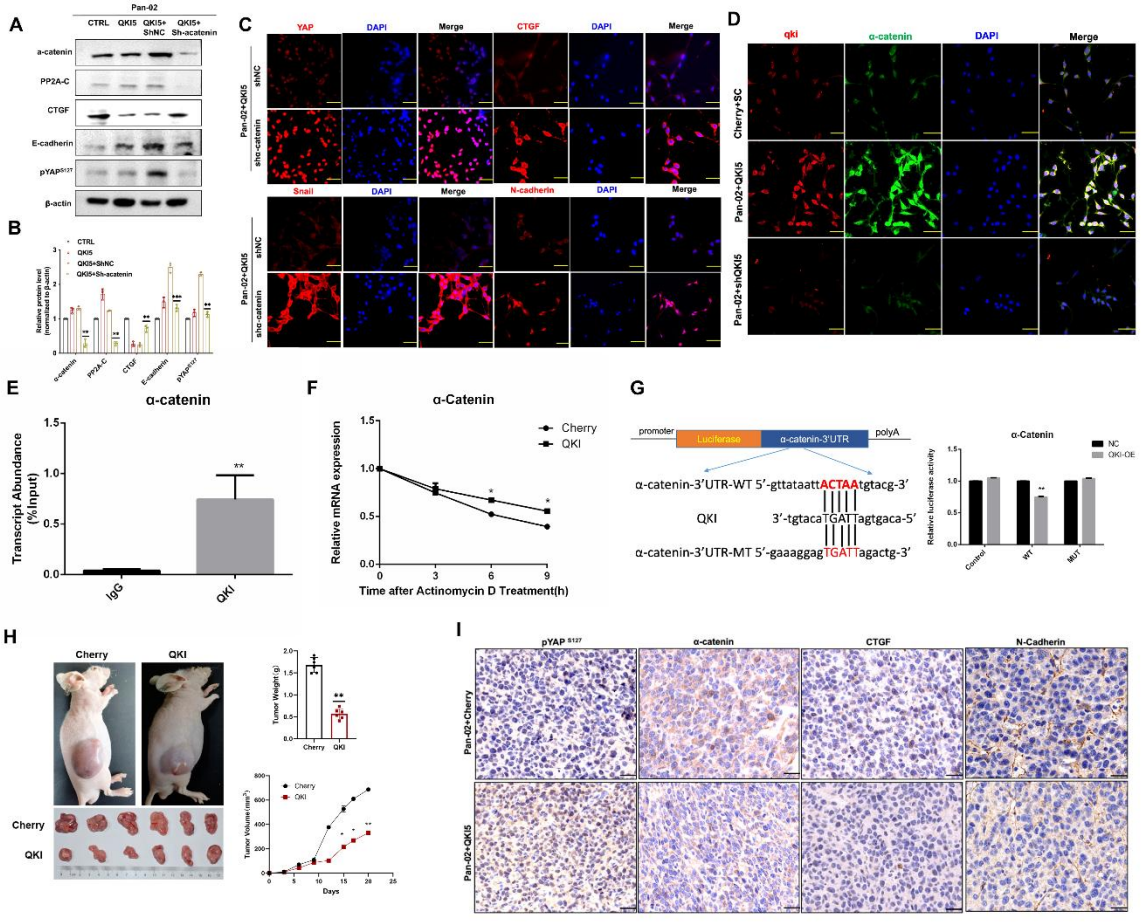


Fig6.2 QKI promotes pYAP^{S127} cytoplasmic localization and inactivation through α-catenin

Fig6.2A-B Western blot analysis of α-catenin, $pYAP^{S127}$ and EMT in Pancreatic tumor cell overexpressed QKI and α-catenin knockdown.

Fig6.2C Immunofluorescence analysis of YAP and EMT in tumor cell of QKI overexpressed and α-catenin knockdown.

Fig6.2D RNA-fish analysis of α-catenin in tumor cell of overexpressing QKI.

Fig6.2E RNA-IP analysis of α-catenin in tumor cell of overexpressing QKI.

Fig6.2F RNA stability analysis of α-catenin in tumor cell of overexpressed QKI.

Fig6.2G RNA reporter analysis of α-catenin in tumor cell of overexpressing QKI.

Fig6.2H The results of tumor volume, weight and morphology in vivo xenograft of tumor cell of overexpressing QKI

Fig6.2I Immunohistochemistry analysis of EMT, α-catenin and $pYAP^{S127}$ in tumor tissue in vivo xenograft

Discussion

PDAC is an aggressive, uniformly lethal disease, characterised by a prominent desmoplastic stroma predominantly composed of a varied assembly of CAFs [28; 29]. While substantial evidence supports the notion that QKI functions as a tumor suppressor, an analysis of the TCGA database surprisingly indicated elevated expression of the QKI RNA-binding protein in PDAC tissues as opposed to normal pancreatic tissue. Intriguingly, further investigation through immunofluorescence and immunohistochemistry of CAFs (identified as sma+ fibroblasts) derived from PDAC patient tissue microarrays, as well as from the adjacent normal pancreas, revealed upregulation of QKI within CAFs, with a distinct localisation to the tumor microenvironment in PDAC samples compared to those from healthy pancreatic tissue.

Based on these findings, we posit that QKI operates as a dual-role molecule within the epithelium and stroma of pancreatic tumors, influencing disease progression through complex interactions(Figure S6).

CAFs are instrumental in facilitating tumor growth and progression through multiple mechanisms. They secrete a diverse array of chemokines and cytokines that modulate the tumuor microenvironment and promote inflammation. Additionally, CAFs contribute to enhanced angiogenesis, provide tumors with the necessary

blood supply for growth, and play a critical role in ECM remodelling, which can facilitate tumor cell migration, invasion, and metastasis. Specifically, HSF1 is often activated in CAFs, which promotes malignancy [30]. Other factors, such as colony-stimulating factor 1 (CSF-1) [31], interleukin-6 (IL-6) [32], connective tissue growth factor (CTGF) [33; 34], leukaemia inhibitory factor(LIF) [35], and matrix metalloproteinases (MMPS) [36], are also secreted by CAFs, further contributing to the tumorigenic process. These molecules not only directly affect cancer cell behaviour, but also indirectly influence other cells within the tumor microenvironment, creating a supportive niche for cancer progression and therapeutic resistance.

Initially, we investigated the potential of QKI to regulate the characteristics and activation of CAFs. Silencing of QKI in CAFs demonstrated significant effects, as it not only curbed the proliferation, migration, invasion, and tumorigenic capabilities of PDAC cells but also induced apoptosis in carcinoma cells through paracrine mechanisms, as shown in Figure 3. These promising in vitro outcomes prompted us to extend our study to in vivo conditions. Subsequently, by employing tumor-bearing and metastasis models in mice, as well as transplantation assays, our experiments with QKI-knockout CAFs consistently revealed a marked reduction in tumor formation. These findings underscore the pivotal role of QKI in the activation of CAFs and the subsequent promotion of tumorigenesis, highlighting its potential as a therapeutic target for PDAC.

Some reports have elucidated the crucial role of YAP activity in sustaining the pro-tumorigenic phenotypes of CAFs, which encompasses matrix stiffening, facilitation of cancer cell invasion, and angiogenesis [37; 38]. Augmented matrix stiffness, a characteristic of the tumor microenvironment, can trigger the activation of the FAK [39] and SRC [40] families of kinases, thereby amplifying YAP transcriptional regulatory activity. This signaling cascade is instrumental in oncogenesis and augmentation of cell stemness. Moreover, the use of FAK and SRC inhibitors in our study also suppressed the Y357 phosphorylation of YAP, a critical event in CAF activation, as depicted in Figure 5.1. Studies have shown that FAK interacts

with SRC kinase to regulate focal adhesions, leading to cytoskeletal reorganization, cell survival, and migration [41].

Our findings align with the GO enrichment and KEGG pathway analyses derived from the mass spectrometry data of LX-2 cells with altered QKI expression levels, as depicted in Figure 5.2A-E. Through a combination of mass spectrometry and TCGA database analysis, we identified three specific target genes: TNC, ITGAV, and PPP2R5E, which are potentially modulated by QKI. This discovery expands our understanding of the molecular mechanisms underlying the influence of QKIs on cellular functions and their potential role in cancer progression.

Tenascin C (TNC), a glycoprotein component of the ECM, is known for its ability to withstand mechanical stress, thereby bestowing tissues with elasticity and structural integrity. TNC's role in disease is significant, with recognised contributions to cardiac and arterial damage, as well as its pivotal role in tumor angiogenesis and metastasis [42, 43, 44]. A previous study showed that TNC, a large glycoprotein located in the ECM, is secreted primarily by CAFs in PDAC [45]. For instance, a recent study reported that high TNC-CAFs play a crucial role in tumor progression and resistance to ICI therapy in patients with PAAD [46]. ITGAV is a crucial component of the integrin family and consists of widely expressed heterodimeric cell-surface receptors that interact with the ECM. These receptors are pivotal in mediating cell adhesion, migration, and signaling processes fundamental to cellular behaviour and tissue homeostasis. In PDAC, ITGAV promotes malignant biological properties in both CAFs and pancreatic cancer cells. The interaction of ITGAV with its ECM ligands can activate downstream signaling pathways that promote tumor growth, invasion, and resistance to therapy [47]. Prior research has indicated that the integrin subunit ITGAV plays a significant role in the progression of malignant characteristics in both CAFs and pancreatic cancer cells in PDAC [48]. PP2A is the predominant enzyme in the serine-threonine phosphatase family and exhibits crucial regulatory functions in various cellular processes, including cell growth, differentiation, and apoptosis [49]. PP2A is highly upregulated in SCLC suggesting that it plays an important role in driving tumorigenesis [50]. Consequently, these three genes are potential targets for QKI

regulation and may play significant roles in the molecular pathways influenced by QKI.

Ultimately, RNA-IP assays and luciferase reporter experiments provided definitive evidence of a direct interaction between QKI and the 3'-untranslated region (UTR) of TNC. These findings establish that TNC is a bonafide target gene of QKI.

Our study demonstrates that QKI has distinct roles in pancreatic cancer cells and CAFs. In CAFs, the high expression level of QKI through direct interaction with TNC activates the FAK/SRC signaling pathway, which subsequently promotes the phosphorylation of YAP at the Y357 site. This cascade of events may contribute to the activation of the tumor microenvironment and proliferation of tumor cells. In contrast, within tumor cells, the low expression level of QKI leads to the suppression of catenin expression, thereby affecting the phosphorylation of YAP at S127, which may facilitate the occurrence and development of cancer.

Understanding these complex molecular interactions is crucial for devising targeted therapeutic strategies that aim to precisely regulate the tumor microenvironment, potentially offering new avenues for improving cancer treatment outcomes. By delving deeper into the functions of QKI and its interactions with both tumor cells and CAFs, we can better understand the molecular mechanisms of pancreatic cancer and lay a solid foundation for the development of novel therapeutic targets and approaches.

Conclusions

Our study provides novel insights into the dual roles of QKI in pancreatic ductal adenocarcinoma (PDAC), highlighting its distinct functions within cancer-associated fibroblasts (CAFs) and tumor cells. In CAFs, elevated QKI expression directly interacts with tenascin C (TNC), activating the FAK/SRC signaling pathway and promoting YAP phosphorylation at Y357. This cascade enhances the pro-tumorigenic activity of CAFs, contributing to the activation of the tumor microenvironment and tumor cell proliferation. Conversely, in tumor cells, low QKI expression suppresses catenin expression, affecting YAP phosphorylation at S127 and promoting cancer progression. These findings underscore the complexity of

QKI's role in PDAC and its potential as a therapeutic target. By targeting QKI and its downstream pathways, we may be able to modulate the tumor microenvironment and improve treatment outcomes for PDAC patients. Further research is warranted to explore the therapeutic potential of QKI modulation and its impact on the intricate molecular interactions within the PDAC microenvironment.

Declarations

Ethics approval and consent to participate

All animal experiments were approved by the Institutional Animal Care and Use Committee of the Fourth Military Medical University(Approval No:IACUC-20241370). All procedures were performed in accordance with the Regulations for the Administration of Affairs Concerning Experimental Animals (China, 1988, revised 2017), the Guide for the Care and Use of Laboratory Animals published by the US National Institutes of Health (NIH publication no. 85-23, revised 1996), and institutional regulations. All efforts were made to minimize animal suffering and to reduce the number of animals used.

Consent for publication

Not applicable to this study.

Availability of data and materials

Genomic Data Commons (GDC) Data Portal (https://portal.gdc.cancer.gov/). We express our deepest appreciation for their support and camaraderie.

Competing interests

The authors have no competing interests.

Funding

The Medical Enhancement Program, Grant/Award Number: 2020SWAQ06. Incubation fund of Shaanxi Provincial People's Hospital, Grant/Award Number:2023YJY-15.

Authors' contributions

Conceptualization, Z.L and G.C.; methodology, Y.B, and D.Z; Investigation, G.C., and D.Z; writing—original draft, G.C. and W.Z.; writing—review & editing, G.C and Z.L.; funding acquisition, Z.L and G.C.; resources, Y.B.; supervision, Z.L.

Acknowledgements

The authors would like to extend our sincere gratitude to all my colleagues in the State Key Laboratory of Cancer Biology， Department of Biopharmaceutics， Fourth military Medical University, Xi'an,China for their invaluable support and assistance throughout the research process. Their selfless dedication, insightful discussions, and team spirit during the experiments have been instrumental to the success of this study. Without their collective efforts, this research would not have been possible. Special thanks go to Tianshu Du, Zhao Yan,Yu Zheng, Di Wei, Zichen Ye, Di Qu, Yan Zhao, Huanyu Lu and Bing Dai. Additionally, We are grateful to Yukui Shang(Tsinghua University)for his invaluable guidance and expertise in data a nalysis.

References

[1] R.L. Siegel, A.N. Giaquinto, and A. Jemal, Cancer statistics, 2024. CA Cancer J Clin 74 (2024) 12-49.

[2] N. Vázquez-Bellón, N. Martínez-Bosch, P. García de Frutos, and P. Navarro, Hallmarks of pancreatic cancer: spotlight on TAM receptors. EBioMedicine 107 (2024) 105278.

[3] D. Ansari, B. Tingstedt, B. Andersson, F. Holmquist, C. Sturesson, C. Williamsson, A. Sasor, D. Borg, M. Bauden, and R. Andersson, Pancreatic cancer: yesterday, today and tomorrow. Future Oncol 12 (2016) 1929-46.

[4] L.D. Wood, M.I. Canto, E.M. Jaffee, and D.M. Simeone, Pancreatic Cancer: Pathogenesis, Screening, Diagnosis, and Treatment. Gastroenterology 163 (2022) 386-402.e1.

[5] V.L. Veenstra, A. Garcia-Garijo, H.W. van Laarhoven, and M.F. Bijlsma, Extracellular Influences: Molecular Subclasses and the Microenvironment in Pancreatic Cancer. Cancers (Basel) 10 (2018).

[6] Y. Miyai, N. Esaki, M. Takahashi, and A. Enomoto, Cancer-associated fibroblasts that restrain cancer progression: Hypotheses and perspectives. Cancer Sci 111 (2020) 1047-1057.

[7] N. Ershaid, Y. Sharon, H. Doron, Y. Raz, O. Shani, N. Cohen, L. Monteran, L. Leider-Trejo, A. Ben-Shmuel, M. Yassin, M. Gerlic, A. Ben-Baruch, M. Pasmanik-Chor, R. Apte, and N. Erez, NLRP3 inflammasome in fibroblasts links tissue damage with inflammation in breast cancer progression and metastasis. Nat Commun 10 (2019) 4375.

[8] Y. Mitsui, N. Tomonobu, M. Watanabe, R. Kinoshita, I.W. Sumardika, C. Youyi, H. Murata, K.I. Yamamoto, T. Sadahira, A.G.H. Rodrigo, H. Takamatsu, K. Araki, A. Yamauchi, M. Yamamura, H. Fujiwara, Y. Inoue, J. Futami, K. Saito, H. Iioka, E. Kondo, M. Nishibori, S. Toyooka, Y. Yamamoto, Y. Nasu, and M. Sakaguchi, Upregulation of Mobility in Pancreatic Cancer Cells by Secreted S100A11 Through Activation of Surrounding Fibroblasts. Oncol Res 27 (2019) 945-956.

[9] C.J. Ko, T.W. Hsu, S.R. Wu, S.W. Lan, T.F. Hsiao, H.Y. Lin, H.H. Lin, H.F. Tu, C.F. Lee, C.C. Huang, M.M. Chen, P.W. Hsiao, H.P. Huang, and M.S. Lee, Inhibition of TMPRSS2 by HAI-2 reduces prostate cancer cell invasion and metastasis. Oncogene 39 (2020) 5950-5963.

[10] T.A. Ebersole, Q. Chen, M.J. Justice, and K. Artzt, The quaking gene product necessary in embryogenesis and myelination combines features of RNA binding and signal transduction proteins. Nat Genet 12 (1996) 260-5.

[11] T.L. Lauriat, L. Shiue, V. Haroutunian, M. Verbitsky, M. Ares, Jr., L. Ospina, and L.A. McInnes, Developmental expression profile of quaking, a candidate gene for schizophrenia, and its target genes in human prefrontal cortex and hippocampus shows regional specificity. J Neurosci Res 86 (2008) 785-96.

[12] C.A. Chénard, and S. Richard, New implications for the QUAKING RNA binding protein in human disease. J Neurosci Res 86 (2008) 233-42.

[13] G. Yang, H. Fu, J. Zhang, X. Lu, F. Yu, L. Jin, L. Bai, B. Huang, L. Shen, Y. Feng, L. Yao, and Z. Lu, RNA-binding protein quaking, a critical regulator of

colon epithelial differentiation and a suppressor of colon cancer. Gastroenterology 138 (2010) 231-40.e1-5.

[14] Y. Zhao, G. Zhang, M. Wei, X. Lu, H. Fu, F. Feng, S. Wang, W. Lu, N. Wu, Z. Lu, and J. Yuan, The tumor suppressing effects of QKI-5 in prostate cancer: a novel diagnostic and prognostic protein. Cancer Biol Ther 15 (2014) 108-18.

[15] F. Yu, L. Jin, G. Yang, L. Ji, F. Wang, and Z. Lu, Post-transcriptional repression of FOXO1 by QKI results in low levels of FOXO1 expression in breast cancer cells. Oncol Rep 31 (2014) 1459-65.

[16] Y. Bian, L. Wang, H. Lu, G. Yang, Z. Zhang, H. Fu, X. Lu, M. Wei, J. Sun, Q. Zhao, G. Dong, and Z. Lu, Downregulation of tumor suppressor QKI in gastric cancer and its implication in cancer prognosis. Biochem Biophys Res Commun 422 (2012) 187-93.

[17] N. Ferrari, R. Ranftl, I. Chicherova, N.D. Slaven, E. Moeendarbary, A.J. Farrugia, M. Lam, M. Semiannikova, M.C.W. Westergaard, J. Tchou, L. Magnani, and F. Calvo, Dickkopf-3 links HSF1 and YAP/TAZ signaling to control aggressive behaviours in cancer-associated fibroblasts. Nat Commun 10 (2019) 130.

[18] Z. Pan, Y. Tian, B. Zhang, X. Zhang, H. Shi, Z. Liang, P. Wu, R. Li, B. You, L. Yang, F. Mao, H. Qian, and W. Xu, YAP signaling in gastric cancer-derived mesenchymal stem cells is critical for its promoting role in cancer progression. Int J Oncol 51 (2017) 1055-1066.

[19]. Ferreira, R. and N. Hein, Purification of Mouse Embryonic Fibroblasts (MEFs). Current protocols, 2023. 3(11): p. e921.

[20]. Zebisch, K., et al., Protocol for effective differentiation of 3T3-L1 cells to adipocytes. Analytical biochemistry, 2012. 425(1): p. 88-90.

[21]. Yuan, L., et al., Isolation of a novel gene, TSP50, by a hypomethylated DNA fragment in human breast cancer. Cancer research, 1999. 59(13): p. 3215-3221.

[22]. Franken, N.A.P., et al., Clonogenic assay of cells in vitro. Nature protocols, 2006. 1(5): p. 2315-2319.

[23] R.F. Hwang, T. Moore, T. Arumugam, V. Ramachandran, K.D. Amos, A. Rivera, B. Ji, D.B. Evans, and C.D. Logsdon, Cancer-associated stromal fibroblasts promote pancreatic tumor progression. Cancer Res 68 (2008) 918-26.

[24]. Kanehisa, M., et al., KEGG: biological systems database as a model of the real world. Nucleic acids research, 2025. 53(D1): p. D672-D677.

[25]. Kanehisa, M. and S. Goto, KEGG: kyoto encyclopedia of genes and genomes. Nucleic acids research, 2000. 28(1): p. 27-30.

[26] H. Wei, Z. Xu, F. Liu, F. Wang, X. Wang, X. Sun, and J. Li, Hypoxia induces oncogene yes-associated protein 1 nuclear translocation to promote pancreatic ductal adenocarcinoma invasion via epithelial-mesenchymal transition. Tumor Biol 39 (2017) 1010428317691684.

[27] Y. Yuan, D. Li, H. Li, L. Wang, G. Tian, and Y. Dong, YAP overexpression promotes the epithelial-mesenchymal transition and chemoresistance in pancreatic cancer cells. Mol Med Rep 13 (2016) 237-42.

[28] E. Karamitopoulou, Tumor microenvironment of pancreatic cancer: immune landscape is dictated by molecular and histopathological features. Br J Cancer 121 (2019) 5-14.

[29] B.Y. Tew, C. Legendre, G.C. Gooden, K.N. Johnson, R.A. Martinez, J. Kiefer, M. Bernstein, J. Glen, L. Butry, A. Hinek, S.A. Toms, and B. Salhia, Isolation and characterization of patient-derived CNS metastasis-associated stromal cell lines. Oncogene 38 (2019) 4002-4014.

[30] R. Scherz-Shouval, S. Santagata, M.L. Mendillo, L.M. Sholl, I. Ben-Aharon, A.H. Beck, D. Dias-Santagata, M. Koeva, S.M. Stemmer, L. Whitesell, and S. Lindquist, The reprogramming of tumor stroma by HSF1 is a potent enabler of malignancy. Cell 158 (2014) 564-78.

[31] V. Kumar, L. Donthireddy, D. Marvel, T. Condamine, F. Wang, S. Lavilla-Alonso, A. Hashimoto, P. Vonteddu, R. Behera, M.A. Goins, C. Mulligan, B. Nam, N. Hockstein, F. Denstman, S. Shakamuri, D.W. Speicher, A.T. Weeraratna, T. Chao, R.H. Vonderheide, L.R. Languino, P. Ordentlich, Q. Liu, X. Xu, A. Lo, E. Puré, C. Zhang, A. Loboda, M.A. Sepulveda, L.A. Snyder, and D.I. Gabrilovich, Cancer-Associated Fibroblasts Neutralize the Anti-tumor Effect

of CSF1 Receptor Blockade by Inducing PMN-MDSC Infiltration of Tumors. Cancer Cell 32 (2017) 654-668.e5.

[32] E. Elyada, M. Bolisetty, P. Laise, W.F. Flynn, E.T. Courtois, R.A. Burkhart, J.A. Teinor, P. Belleau, G. Biffi, M.S. Lucito, S. Sivajothi, T.D. Armstrong, D.D. Engle, K.H. Yu, Y. Hao, C.L. Wolfgang, Y. Park, J. Preall, E.M. Jaffee, A. Califano, P. Robson, and D.A. Tuveson, Cross-Species Single-Cell Analysis of Pancreatic Ductal Adenocarcinoma Reveals Antigen-Presenting Cancer-Associated Fibroblasts. Cancer Discov 9 (2019) 1102-1123.

[33] Y. Ohara, S.H. Chew, N. Misawa, S. Wang, D. Somiya, K. Nakamura, H. Kajiyama, F. Kikkawa, Y. Tsuyuki, L. Jiang, K. Yamashita, Y. Sekido, K.E. Lipson, and S. Toyokuni, Connective tissue growth factor-specific monoclonal antibody inhibits growth of malignant mesothelioma in an orthotopic mouse model. Oncotarget 9 (2018) 18494-18509.

[34] Y.W. Shen, Y.D. Zhou, H.Z. Chen, X. Luan, and W.D. Zhang, Targeting CTGF in Cancer: An Emerging Therapeutic Opportunity. Trends Cancer 7 (2021) 511-524.

[35] G. Biffi, T.E. Oni, B. Spielman, Y. Hao, E. Elyada, Y. Park, J. Preall, and D.A. Tuveson, IL1-Induced JAK/STAT Signaling Is Antagonized by TGFβ to Shape CAF Heterogeneity in Pancreatic Ductal Adenocarcinoma. Cancer Discov 9 (2019) 282-301.

[36] V. Plaks, N. Kong, and Z. Werb, The cancer stem cell niche: how essential is the niche in regulating stemness of tumor cells? Cell Stem Cell 16 (2015) 225-38.

[37] T. Liu, L. Zhou, K. Yang, K. Iwasawa, A.L. Kadekaro, T. Takebe, T. Andl, and Y. Zhang, The β-catenin/YAP signaling axis is a key regulator of melanoma-associated fibroblasts. Signal Transduct Target Ther 4 (2019) 63.

[38] M.J. Paszek, N. Zahir, K.R. Johnson, J.N. Lakins, G.I. Rozenberg, A. Gefen, C.A. Reinhart-King, S.S. Margulies, M. Dembo, D. Boettiger, D.A. Hammer, and V.M. Weaver, Tensional homeostasis and the malignant phenotype. Cancer Cell 8 (2005) 241-54.

[39] H.J. Wu, M. Hao, S.K. Yeo, and J.L. Guan, FAK signaling in cancer-associated fibroblasts promotes breast cancer cell migration and metastasis by exosomal miRNAs-mediated intercellular communication. Oncogene 39 (2020) 2539-2549.

[40] M. Kakarla, S. ChallaSivaKanaka, M.F. Dufficy, V. Gil, Y. Filipovich, R. Vickman, S.E. Crawford, S.W. Hayward, and O.E. Franco, Ephrin B Activate Src Family Kinases in Fibroblasts Inducing Stromal Remodeling in Prostate Cancer. Cancers (Basel) 14 (2022).

[41] M.J. Oudin, O. Jonas, T. Kosciuk, L.C. Broye, B.C. Guido, J. Wyckoff, D. Riquelme, J.M. Lamar, S.B. Asokan, C. Whittaker, D. Ma, R. Langer, M.J. Cima, K.B. Wisinski, R.O. Hynes, D.A. Lauffenburger, P.J. Keely, J.E. Bear, and F.B. Gertler, Tumor Cell-Driven Extracellular Matrix Remodeling Drives Haptotaxis during Metastatic Progression. Cancer Discov 6 (2016) 516-31.

[42] L. Zheng, D. Zhang, Y. Zhang, Y. Wen, and Y. Wang, mTOR signal transduction pathways contribute to TN-C FNIII A1 overexpression by mechanical stress in osteosarcoma cells. Mol Cells 37 (2014) 118-25.

[43] T. Rupp, B. Langlois, M.M. Koczorowska, A. Radwanska, Z. Sun, T. Hussenet, O. Lefebvre, D. Murdamoothoo, C. Arnold, A. Klein, M.L. Biniossek, V. Hyenne, E. Naudin, I. Velazquez-Quesada, O. Schilling, E. Van Obberghen-Schilling, and G. Orend, Tenascin-C Orchestrates Glioblastoma Angiogenesis by Modulation of Pro- and Anti-angiogenic Signaling. Cell Rep 17 (2016) 2607-2619.

[44] K. Imanaka-Yoshida, I. Tawara, and T. Yoshida, Tenascin-C in cardiac disease: a sophisticated controller of inflammation, repair, and fibrosis. Am J Physiol Cell Physiol 319 (2020) C781-c796.

[45] I. Esposito, R. Penzel, M. Chaib-Harrireche, U. Barcena, F. Bergmann, S. Riedl, H. Kayed, N. Giese, J. Kleeff, H. Friess, and P. Schirmacher, Tenascin C and annexin II expression in the process of pancreatic carcinogenesis. J Pathol 208 (2006) 673-85.

[46] S. Furuhashi, Y. Morita, A. Matsumoto, S. Ida, R. Muraki, R. Kitajima, M. Takeda, H. Kikuchi, Y. Hiramatsu, and H. Takeuchi, Tenascin C in pancreatic

cancer-associated fibroblasts enhances epithelial mesenchymal transition and is associated with resistance to immune checkpoint inhibitor. Am J Cancer Res 13 (2023) 5641-5655.

[47] F. Liu, Q. Wu, Z. Dong, and K. Liu, Integrins in cancer: Emerging mechanisms and therapeutic opportunities. Pharmacol Ther 247 (2023) 108458.

[48] T. Wang, J. Yang, J. Mao, L. Zhu, X. Luo, C. Cheng, and L. Zhang, ITGA5 inhibition in pancreatic stellate cells re-educates the in vitro tumor-stromal crosstalk. Med Oncol 40 (2022) 39.

[49] W.D. Dupont, J.P. Breyer, K.M. Bradley, P.A. Schuyler, W.D. Plummer, M.E. Sanders, D.L. Page, and J.R. Smith, Protein phosphatase 2A subunit gene haplotypes and proliferative breast disease modify breast cancer risk. Cancer 116 (2010) 8-19.

[50] G.L. Coles, S. Cristea, J.T. Webber, R.S. Levin, S.M. Moss, A. He, J. Sangodkar, Y.C. Hwang, J. Arand, A.P. Drainas, N.A. Mooney, J. Demeter, J.N. Spradlin, B. Mauch, V. Le, Y.T. Shue, J.H. Ko, M.C. Lee, C. Kong, D.K. Nomura, M. Ohlmeyer, D.L. Swaney, N.J. Krogan, P.K. Jackson, G. Narla, J.D. Gordan, K.M. Shokat, and J. Sage, Unbiased Proteomic Profiling Uncovers a Targetable GNAS/PKA/PP2A Axis in Small Cell Lung Cancer Stem Cells. Cancer Cell 38 (2020) 129-143.e7.

Supplementary Files

This is a list of supplementary files associated with this preprint. Click to download.

- table1.docx